CHAPTER VIII *DISLOCATION KINETICS*

Until now, we have considered dislocations as sources of internal stresses, and their motion results in plastic deformation without focusing on their contribution to plasticity. However, it is clear that plastic deformation results from the displacement of dislocations. Moreover, dislocations encounter and interact with different obstacles when moving within a crystal, e.g., crystal lattice, other dislocations, impurities, and other defects that oppose their motion.

Chapter VIII first aims to clarify how the dislocation motion induces plastic deformation and then discusses and analyzes the mechanisms by which obstacles impede dislocation motion.

8.1 Relation between shear and macroscopic deformation

We have seen in Chapter VI that the displacement of a dislocation line in a crystal sample introduces a deformation, which we described with the Orowan equation:

$$\varepsilon = \Lambda b u$$

The uniaxial tensile (or compressive) test is the most common strain test used, where the strain ε is defined by:

$$\gamma = \frac{dL}{L}$$

where *dL* is the total variation in the length of the sample, and L is its initial length for small plastic deformation. By considering the geometry of the deformation, shear is given by (see Figure 8-1):

$$\varepsilon = \frac{b}{L\cos\phi}$$

and the corresponding strain of the sample is proportional to the following:

$$\gamma = \frac{b\cos\lambda}{L}$$

Finally:

$$\gamma = cos\lambda cos\phi\varepsilon = m\varepsilon \qquad (8.1)$$

The Schmid factor m is the same as described in Chapter VI for stresses (6.1). This equation quantitatively relates the microscopic strain associated with crystal slip and the Burgers vector to the macroscopic strain.

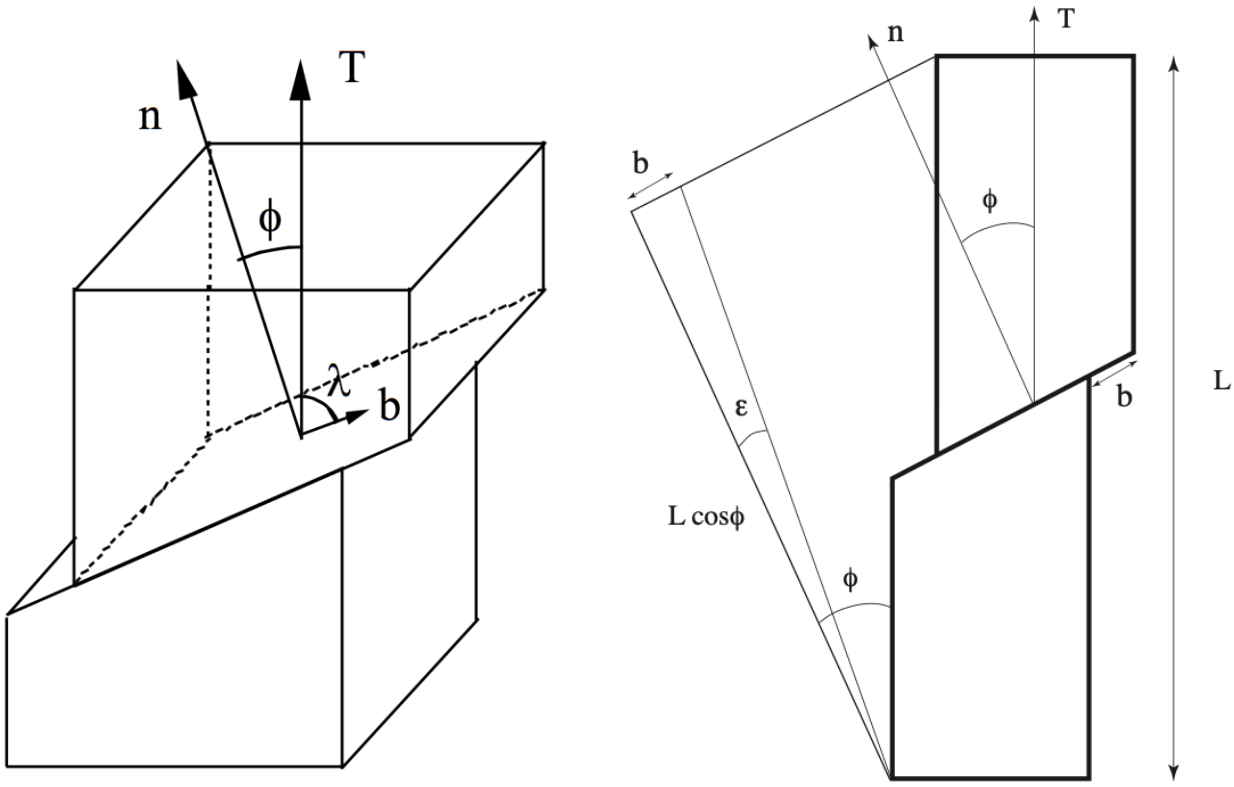

Figure 8-1: *Relation between γ and ε*

Remarks:

- Equivalent expressions exist if the displacement of the dislocation occurs by climb motion.
- We can also see in Figure 8-1 that the translation of the load axis accompanies plastic strain. In the case of a monocrystalline sample, for instance, if the two ends were held rigidly, this would produce a lattice rotation, possibly leading to a non-homogeneous strain.

8.2 Strain curve

We just saw how the displacement of a dislocation induces a deformation, which can be directly related to a macroscopic "measurable" strain. This displacement can be either reversible or irreversible. Moreover, a dislocation can spontaneously create other dislocations by moving across the crystal (e.g., Frank-Read sources). Studying these phenomena involves creating consecutive loading and unloading cycles and measuring the corresponding strains. From this empirical knowledge, we can then identify the different behaviors of dislocations under the action of an external load on a stress-strain curve (Figure 8-2).

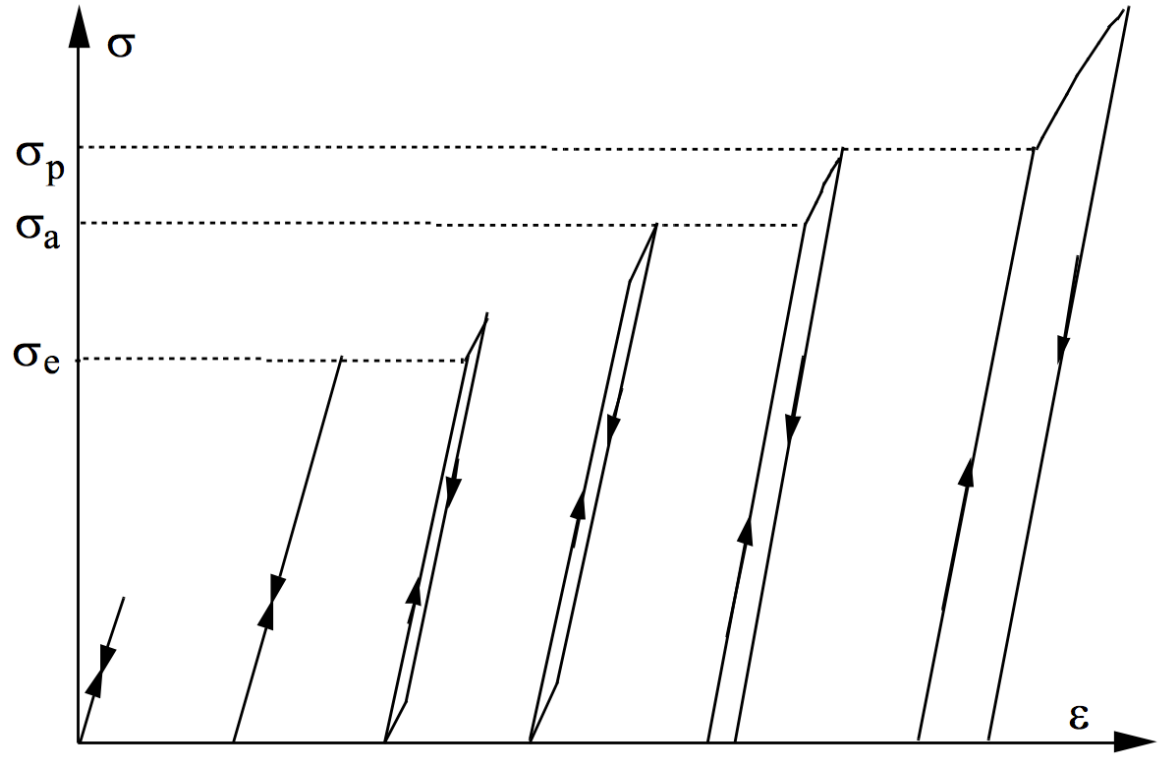

Figure 8-2: *Analysis of a stress-strain curve by repetition of loading-unloading cycles*

Following Brown's terminology, we can identify three kinds of "elastic limits," each corresponding to different dislocation behavior:

- In a purely elastic domain, $\sigma < \sigma_{y,}$ no motion of dislocations occurs.
- An anelastic domain, $\sigma_y < \sigma < \sigma_a$, arises from dislocations bent between their anchor points under stress, restoring their initial position during unloading. That is, this domain corresponds to the reversible motion of dislocations. The phenomena related to anelasticity are described in more detail in chapter X.
- In a microplastic domain, $\sigma_a < \sigma < \sigma_p$, dislocations move over longer distances and can run into obstacles on which they are pinned. Some dislocations' motion is no longer irreversible, and a plastic residual strain is permanent after unloading. For a dislocation density of $\rho \sim 10^9$ m/m^3, this domain can start from a strain $\varepsilon \approx 10^{-6}$, that is to say, for a mean free path of the size of the Frank network, up to a strain of $\varepsilon \sim 10^{-3}$, that is to say for a distance traveled of the size of a monocrystal sample (~cm).
- Lastly, in a plastic domain, $\sigma > \sigma_{p,}$ dislocations move and multiply. It differs from the previous domain in the number and the nature of the mobile dislocations. Furthermore, the multiplication of dislocations requires that all types of dislocations be mobile; this was not obvious in the case where $\sigma < \sigma_p$.

These deformation characteristics and dislocation behavior often correspond to a gradual elastoplastic transition and the difficulty of precisely defining where the plastic domain begins. This is why we frequently define a conventional limit, the engineering yield stress, at which the stress-strain curve is at an arbitrary distance (0.2%) from the tangent to the origin.

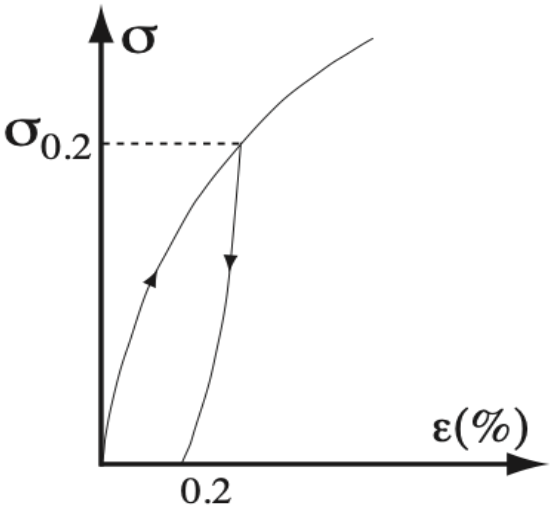

Despite being useful in practice, we must emphasize that this definition has little physical sense and can lead to significant mistakes.

Other, more physical methods exist to define σ_p, for example, by following the evolution of specific physical parameters directly related to the mobility of dislocations as functions of stress (or strain).

We observe, nevertheless, that the stress varies as a function of the strain. Therefore, it is interesting to study the parameters acting upon the displacement velocity of dislocations.

Figure 8-3: *Elastic limit* $\sigma_{0.2}$ *(yield stress)*

We can distinguish four kinds of interactions that can influence the dynamics of dislocations.

i) Interactions with the crystal lattice. The dislocation tends to rearrange along specific crystallographic directions. The dislocation must overcome the "friction" of the lattice to move, which can be described as a periodic potential, which must be overcome during its motion. This interaction is dominant at low temperatures.

ii) Interactions with other dislocations. We have seen in Chapter VII that dislocations can interact between them with forces, which can limit their motion.

iii) Interaction with point defects. Every point defect creates an elastic deformation of the lattice, which can interact with dislocations. On the other hand, the motion of dislocations can cause the displacement of point defects (dragging). The interaction of types ii) and iii) is observed as soon as diffusion and self-diffusion are activated.

iv) Interaction with extended obstacles: precipitates, grain boundaries. Often, overcoming these obstacles requires significant thermal activation. It is a high-temperature phenomenon.

v) Irradiation. We have seen in the electromagnetic analogy that the presence of a dislocation in the elastic medium is analog to the presence of current in space. We can go one step further with this analogy by showing that a dislocation can be subject to relativistic effects, with a "mass" that becomes infinite at the speed of sound (its upper-velocity limit). On the other hand, if a dislocation is accelerated, it radiates photons similarly to an electric charge emitting electromagnetic waves. In the same way, it can also absorb photons, just like a charge in the Compton effect. All these effects can be observed during the excitation by vibration beyond 100 MHz or during ballistic impacts. However, their study is beyond our course objectives. Interested readers can refer to Hirth J. P. and Lothe J.'s "Theory of dislocations" for further details.

8.3 Interactions of dislocations with the crystal lattice

When a dislocation moves by an interatomic distance within a crystal, the atomic arrangement of atoms A, B, and C in the core region varies during the displacement between stable positions (Figure 8-4 a and c). However, the configuration necessarily has a local maximum (Figure 8-4 b).

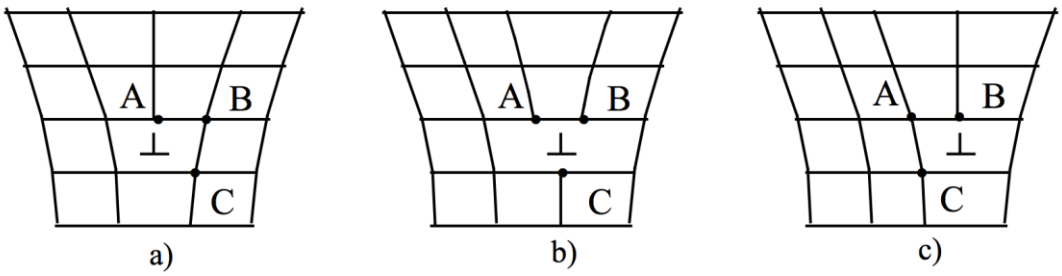

Figure 8-4: *Propagation of a dislocation regulated by the crystal lattice*

This variation of core energy W(x) generates resistance to dislocation glide, called lattice friction or Peierls-Nabarro force. In the presence of a stress σ, the variation in the free energy of the dislocation (see Chapter IX for a justification of the following formula (8.2)) is modified during its motion (Figure 8-5).

$$\Delta G \cong W(x) - \sigma b x \tag{8.2}$$

The stable positions of W(x) in the absence of stress (Figure 8-4a) become metastable positions in the presence of a stress σ (Figure 8-4c). The Peierls-Nabarro stress is the minimum value of σ (at the temperature T=0 K) for which no metastable position (such as S) exists:

$$\left(\frac{\partial W(x)}{\partial x}\right) - \sigma_0 b = 0$$

Following Figure 8-5, we take as potential W(x):

$$W(x) = -\left(\frac{\tau_I - \tau_S}{2}\right)\sin\frac{2\pi x}{a}$$

$$\frac{\partial W(x)}{\partial x} = -\frac{\pi}{a}\left(\frac{\tau_I - \tau_S}{2}\right)\cos\frac{2\pi x}{a}$$

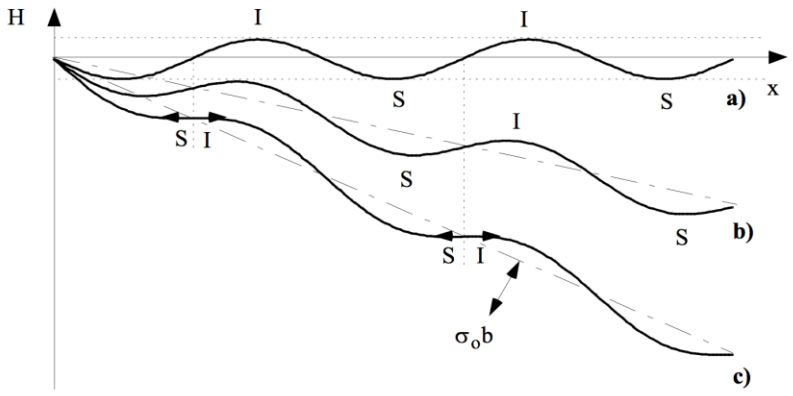

Figure 8-5: *Effect of the applied stress on the potential of the dislocation*

We can then derive σ_0 by considering the points with the horizontal tangent of the potential W(x):

$$\sigma_0 b = \frac{\alpha}{a}(\tau_U - \tau_S) \quad \text{and thus:} \quad \sigma_0 = \frac{\alpha}{ab}(\tau_U - \tau_S) \tag{8.3}$$

where τ_U and τ_S are the dislocation line tension in the unstable and stable positions, respectively. α is a parameter that depends on the shape of W(x): α = 2 if for a linear variation, α = π for a sinusoidal function, such as the one considered here, and α = 4 for a parabolic function.

It is clear that this lattice friction only affects the dislocations that are parallel to the close-packed directions. If the direction of a straight dislocation is different, the average value of the core energy W(x) changes little during the displacement.

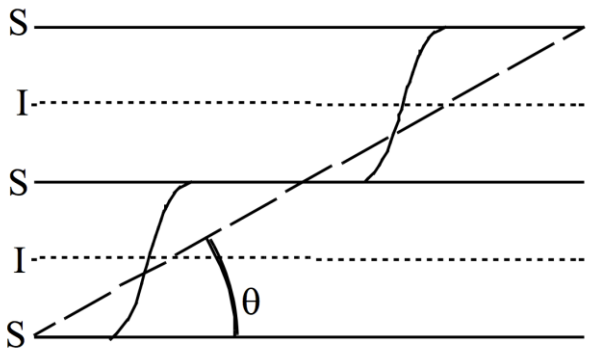

Figure 8-6: *Kinks*

Nevertheless, for energy reasons, such dislocations do not remain straight. Instead, they assume a zig-zag shape, which enables segments of the dislocation line to lie on the dense atomic valleys of the glide plane, lowering their core energy (Figure 8-6). In addition, these segments are linked by kinks of higher energy, in which the lattice friction is generally lower so that they can easily move unless they follow themselves along a close-packed crystallographic direction.

When T≠0 K, the value for the stress σ_0 decreases as long as some coherent atomic fluctuations along the dislocation line (due to thermal agitation) favor the formation of kink pairs (Figure 8-7). Their slow dislocation velocities due to the lattice friction force is a measurable phenomenon at low temperatures. At low-stress values, the formation energy of a pair of kinks, as represented in Figure 8-7, corresponds to one of two already well-formed kinks that the interaction is neglected.

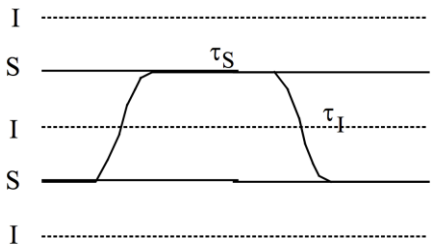

Figure 8-7: *Kink pair*

For aluminum, with μb^3 ~ 1.3 eV, we get the energy of 0.12 eV for a Peierls stress on the order of magnitude of $\mu/1000$.

To summarize, only dislocations parallel to the close-packed lines show significant lattice friction, and the propagation stress increases with temperature because of thermal activation.

8.4 Propagation controlled by the interaction with other dislocations

When the lattice friction is weak, the elastic limit of pure metals is controlled by the interaction between dislocations. These interactions are usually classified into two categories:

- Long-distance interactions with the Frank network, which do not cut the glide plane of the mobile dislocation
- Short-distance interactions with the dislocations that cross the glide plane of the mobile dislocation and to which it directly interacts by forming junctions, jogs, etc. Nevertheless, the dislocations moving through a glide plane containing the mobile dislocation can also cause long-range stress fields, but in the next derivations, we neglect these interactions.

8.4.1 Long-distance stresses due to the Frank network

The dislocations that do not cut the glide plane of the mobile dislocation induce stresses on the glide plane of the mobile dislocation by their stress field. If we consider a certain number of fixed dislocations at an average distance ***l*** (***l*** being the step of the Frank network) and with Burgers vector $\vec{b}$ and $-\vec{b}$, distributed randomly in planes approximatively parallel to the glide plane of the mobile dislocation, the stresses in the glide plane oscillate around a zero mean value with an amplitude σ_m and a two-dimensional wavelength of the order of ***l***.

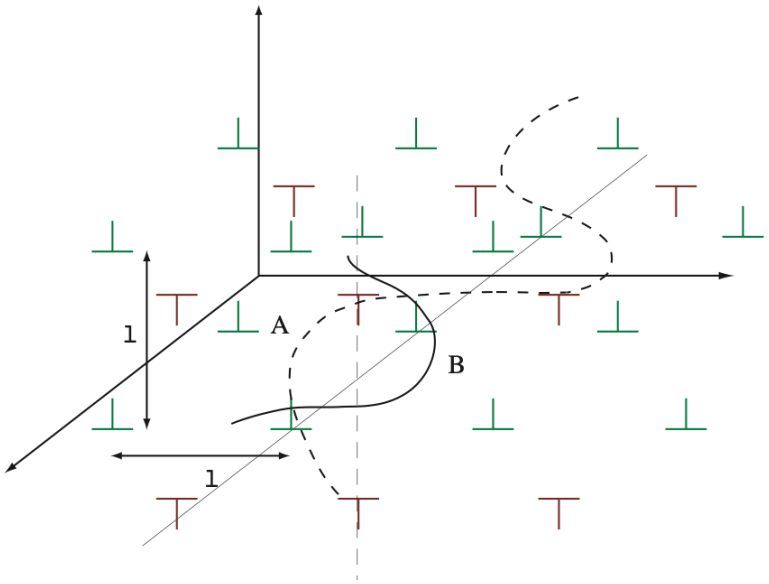

Figure 8-8: *Mobile dislocation in a Frank network with alternating Burgers vectors*

In such a configuration, σ_m is alternatively positive and negative, according to the sign of the Burgers vector (same or opposite sign of the dislocations in the vertical position, see § 7.5.2.c).
The dislocation takes a sinusoidal shape (Figure 8-8). However, for dislocations to move, they must cross regions where σ_m is maximum. Therefore, the gliding only occurs when the stress applied is sufficient to move the dislocation from position A to position B through the maximum stress σ_m (Figure 8-8). The value of σ_m can be estimated by calculating the stress applied on a mobile dislocation by two other identical fixed and parallel dislocations placed roughly symmetrically from one side and the other of the glide plane. Figure 8-9 shows the mobile dislocation located at the origin. We note in equation (7.33) that the stress applied by a mobile edge dislocation in the glide plane by a fixed dislocation is given by:

$$\sigma_{xy} \approx \frac{\mu b}{4\pi K}\frac{\cos\theta cos2\theta}{r}$$

In the current case, the configuration is inverted, and we have two dislocations. The stress is then:

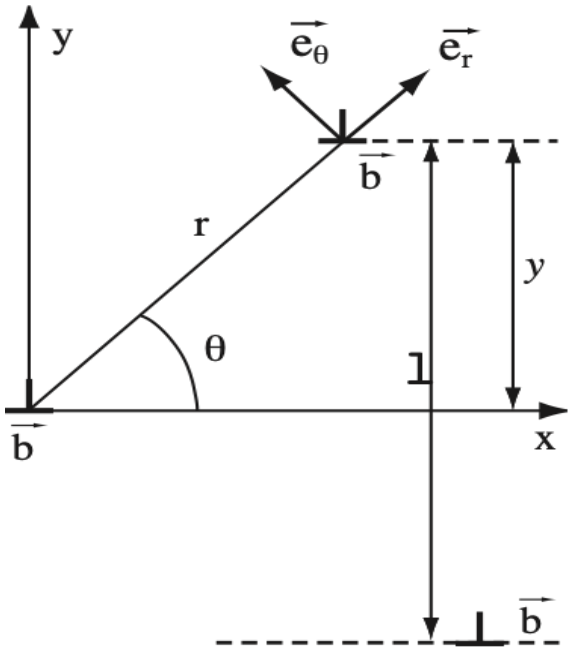

$$\sigma_{xy} \approx -\left(\frac{\mu b}{2\pi K}\right)\frac{\cos\theta\cos 2\theta}{r}$$

That is, with $r = y / sin\theta$:

$$\sigma_{xy} = -\frac{\mu b}{4\pi K}\frac{\sin 2\theta cos2\theta}{y} = -\frac{\mu b}{8\pi K}\frac{\sin 4\theta}{y}$$

which has a maximum for θ=π/8, relatively far from the two fixed dislocations. This indicates that the position of the mobile dislocation is determined by *y* and that it does not have a significant influence, while in fact, only the distance ***l,*** which separates the two fixed dislocations, matters.

Figure 8-9: *Dislocation crossing a plane of two fixed dislocations*

We can then consider a first approximation for the value of σ_m (absolute value), which is given by $\theta = \pi / 8$ and thus:

$$\sigma_m \approx \frac{\mu b}{8\pi K}\left(\frac{1}{y}+\frac{1}{l-y}\right)$$

$$\sigma_m \approx \frac{\mu b}{8\pi Kl}\left(\frac{l^2}{y(l-y)}\right) = \frac{\mu b}{8\pi Kl}\left(\frac{l}{y\left(1-(y/l)\right)}\right)$$

from which
that is - letting *Y=y/l:*

$$\sigma_m \approx \frac{\mu b}{2\pi Kl}\left(\frac{1}{4Y(1-Y)}\right) = \left(\frac{\mu b}{2\pi Kl}\right) f(Y)$$

and we can thus consider for $0.3 \leq Y \leq 0.7$ (Figure 8-10):

$$\sigma_m \approx \frac{\mu b}{2\pi K l}$$

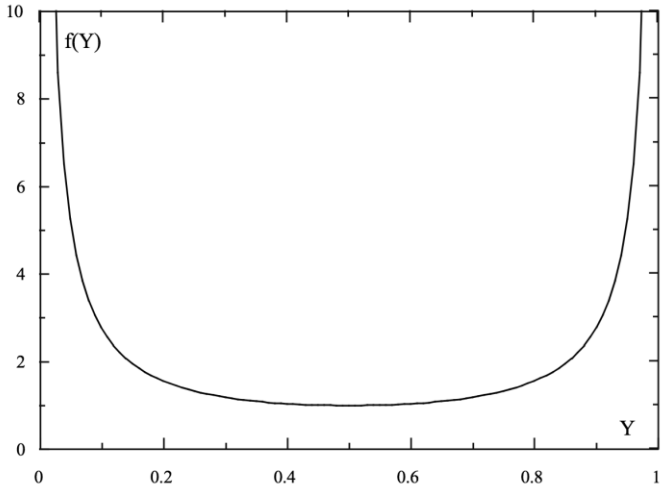

Figure 8-10: *Interaction stress between the overlapped dislocations*

In fact, from $Y \leq 0.3$ or $Y \geq 0.7$, the stress σ_m steeply becomes large, and the dislocation cannot pass, meaning that the force is high if one of the dislocations is close to the plane of the mobile dislocation and low if y is close to ***l***/2 (Y=1/2).

8.4.2 Short-distance interactions

Short-distance interactions occur with dislocations that cut the glide plane of the mobile dislocation, with which this can interact. Three possible types of interactions exist. First, the dislocations cutting the glide plane are referred to as the "trees" of the forest, which can be either attractive or repulsive or without elastic interactions with the mobile dislocation. However, regardless of the type of situation, the final configuration generally requires the formation of two jogs (Figure 8-11), one on the mobile dislocation and the other on the tree (each one of the jogs corresponds respectively to the Burgers vectors of the intersected dislocation). Their formation requires some energy reaching to a stress σ, which we can initially neglect for attractive and repulsive trees, but not for trees without elastic interaction, where this energy becomes then dominating.

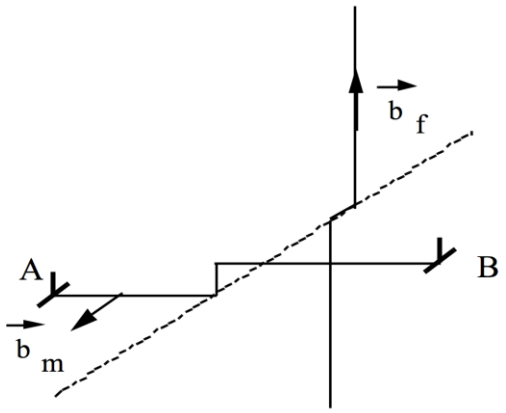

Figure 8-11: *Dislocation jogs formed during an intersection*

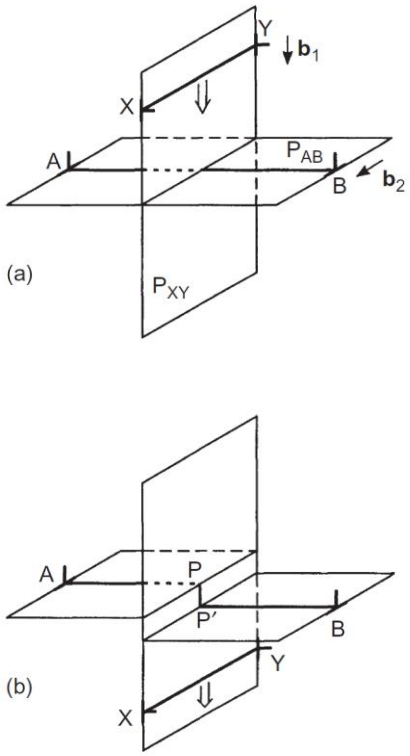

a) The intersection of edge dislocations with perpendicular Burgers vectors

A dislocation XY with Burgers vector $\vec{b_1}$ moves in the plane P_{XY} and cuts the dislocation AB with Burgers vector $\vec{b_2}$. Since the atoms on one side of the P_{XY} plane are displaced by an atomic row with respect to the atoms lying on the other side when XY crosses the intersection, a jog PP' is created on the dislocation AB.

The jog maintains the Burgers vector of AB $\vec{b_2}$, which has a length b_1. Therefore, we cannot form a jog on dislocation XY because $\vec{b_2}$ is parallel to XY.

Since the energy per unit length of a dislocation is approximatively equal to $\alpha\mu b^2$, the energy of the jog is roughly equivalent to $\alpha\mu b^3$.

Figure 8-12: *Intersection between two edge dislocations with perpendicular Burgers vectors*

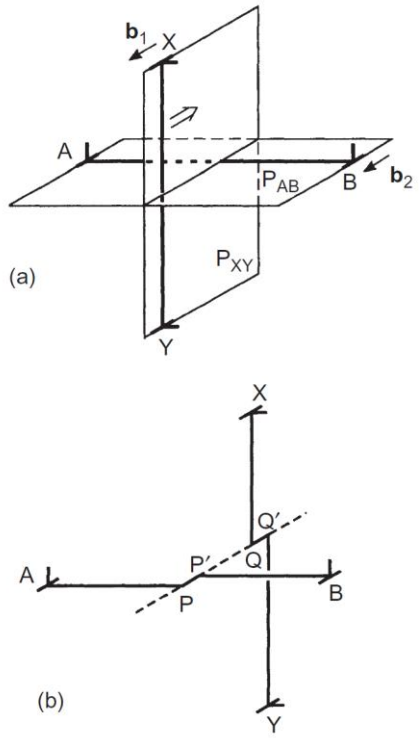

b) Intersection of edge dislocations with parallel Burgers vectors

The intersection of two edge dislocations with parallel Burgers vectors is shown in Figure 8-13. Again, a jog in each dislocation is formed.

Figure 8-13: *Intersection of two edge dislocations with parallel Burgers vectors*

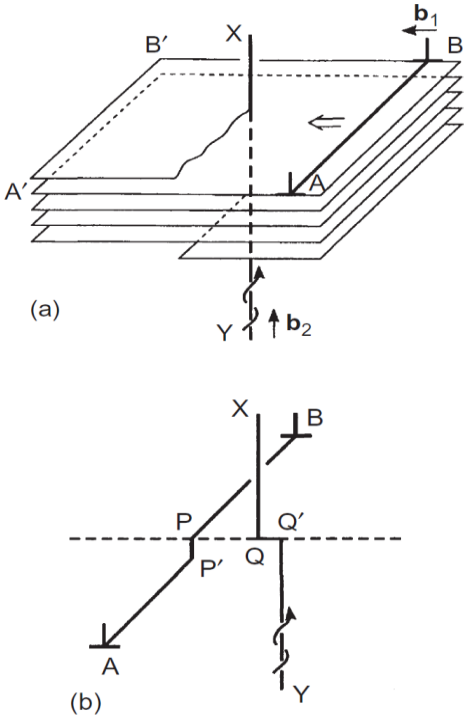

c) Intersection of an edge dislocation with a screw dislocation

The arrangement of atomic planes in the crystal near the screw dislocation is shaped like a spiral.

After crossing the screw dislocation, the ends of the edge dislocation are not in the same plane anymore: the dislocation forms then a jog parallel to the screw dislocation. On the other hand, as in the previous cases, the edge dislocation creates a jog on the screw dislocation.

Figure 8-14: *Intersection of an edge dislocation with a screw dislocation*

d) Attractive tree

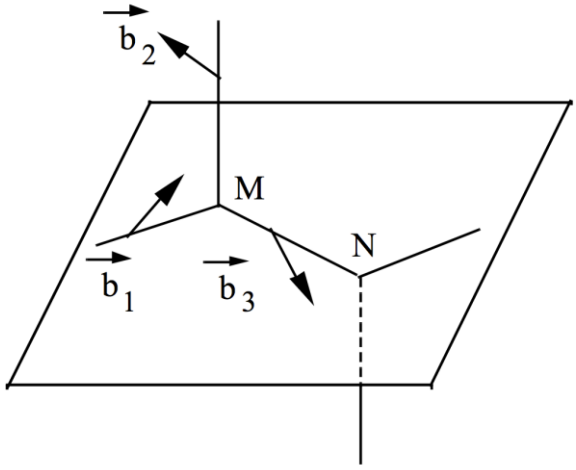

A tree with Burgers vector $\vec{b_2}$ is called attractive when a mobile dislocation with Burgers vector $\vec{b_1}$ reacts with it to form a dislocation with Burgers vector $\vec{b_3}$, which is the sum of the Burgers vectors $\vec{b_3} = \vec{b_1} + \vec{b_2}$ such that $b_3^2 < b_2^2 + b_1^2$.
In this case, the two dislocations combine over some length MN starting at the intersection of the two respective planes of the two dislocations so that the line energy is decreased (Figure 8-15).

Figure 8-15 : *Formation of a common segment MN during the interaction with an attractive tree*

e) Repulsive tree

If the dislocations stayed straight, the stresses required to cut a "repulsive" or "attractive" tree would be the same. However, the rearrangements at the intersection of the two dislocations increase the interaction energy of the "attractive" trees and decrease the interaction energy of the repulsive trees to stabilize the system. However, the repulsive trees cause less significant hardening; thus, we don't provide further explanation in this Chapter's context.

8.5 Propagation controlled by the interaction with a solid solution

The mechanical properties of metals are generally modified by alloying elements producing atomic-level defects, e.g., substitutional or interstitial-type. Alloying solute elements typically make the material harder, indicating that they obstruct dislocation motion. The interactions can differ according to the nature of these alloy elements. However, it is still possible to find one general formulation for hardening based on determining an obstacle's force coupled with a statistical method.

The following presents different possible interactions between the dislocations and these impurities. We assume at first that they are fixed, i.e., the temperature is sufficiently low so that diffusion is negligible.

8.5.1 Types of interaction between dislocations and atoms of the solute

a) Size effect

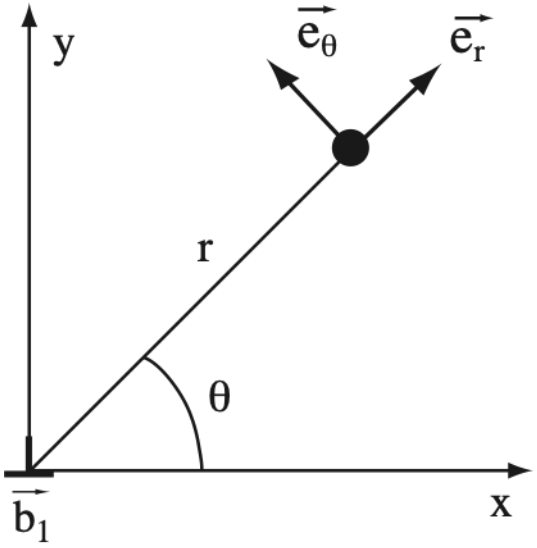

In the case of an impurity with a spherical symmetry, it can be considered that its introduction in the crystal lattice causes a volume change. The associated stress tensor is then equivalent to hydrostatic pressure.

We have seen (Chapter III) that any stress state can be split into its shear components (the trace of the tensor is zero) and a hydrostatic pressure component, which acts on the volume change, that is:

$$\sigma_p = \frac{1}{3}(\sigma_{11} + \sigma_{22} + \sigma_{33}) = \frac{1}{3}Tr(\sigma)$$

Figure 8-16: *Interaction geometry of a point defect with a dislocation*

Thus, a straight edge dislocation applies at the point (r, θ) a hydrostatic pressure on the impurity (see equation (7.14)):

$$p = \frac{1}{3}\sigma_{ii} = -\frac{1}{3\pi}\frac{(1+\nu)}{(1-\nu)}\frac{\mu b sin\theta}{r} \tag{8.4}$$

As a consequence, neglecting the internal energy of the impurity and inserting a spherical impurity of volume ’Ω=Ω+ηΩ in a cavity with a volume equal to an atomic volume Ω, energy must be applied against the stress field of the dislocation to displace it from infinity to a position *r* with respect to the dislocation:

$$W_I = p\eta\Omega = -\frac{1}{3\pi}\frac{(1+\nu)}{(1-\nu)}\frac{\mu b\eta\Omega\sin\theta}{r} \tag{8.5}$$

which constitutes the energy of the interaction with the dislocation. This energy is supplied by the dislocation (the system). If it is positive, the system's energy decreases; if it is negative, the energy of the system increases.

If $\eta < 0$ (solute is smaller than solvent atoms), the impurity goes preferentially in the compressed zone (= zone of the extra half-plane) of the dislocation. If $\eta > 0$ (solute bigger), it tends to migrate to the dilatation zone.

The maximum interaction energy (it is binding energy, which is thus negative) is given for $\theta = \pi/2$ and $r \sim 2b/3$, that is to say, when the impurity is in the core of the dislocation:

$$W_I = -\frac{1}{2\pi}\frac{(1+\nu)}{(1-\nu)}\mu|\eta|\Omega \sim -\frac{1}{\pi}\mu|\eta|\Omega$$

An impurity located at a height y of the glide plane of a dislocation applies a force on it given by:

$$F = -\left.\frac{\partial W_I}{\partial x}\right|_y = \frac{\mu b \eta V}{3\pi}\frac{(1+\nu)}{(1-\nu)}\frac{xy}{(x^2+y^2)^2}$$

Remark:

Since the hydrostatic pressure linked to a perfect screw dislocation is zero in isotropic linear elasticity, this dislocation is not affected by the size effect of impurity with spherical symmetry.

b) Tetragonal effect

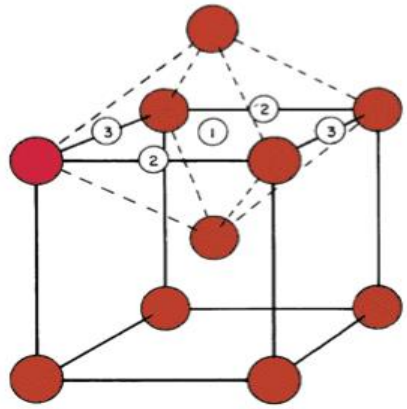

In reality, impurities (particularly interstitial impurities) cause an antisymmetric distortion and do not generally function as a simple expansion center. As a result, the elastic displacements do not have spherical symmetry but rather exhibit tetragonal symmetry (the case of carbon atoms in a solid solution in iron). In this case, the impurity also interacts with the shear stresses of the dislocation, leading to an additional energy term, which in this case, affects screw dislocations as well.

Figure 8-17: *Carbon atoms are located on octahedral sites.*

c) Modulus effect

Because the elastic constants are higher or lower around the impurity than in the matrix, more or less elastic energy is stored in the stress field of the dislocation. All this corresponds to an attraction or repulsion by the impurity, according to the sign of the modulus effect. Although this effect is generally weaker than those mentioned previously, it can be important when there is a high elastic modulus variation (case of vacancies where $\mu_L = 0$). Other effects exist, such as the electrostatic effect, dissociation, etc.

To summarize very briefly:

$$W_{tetragonal} > W_{size} > W_{module} > W_{electrostatic}$$

Knowing the energy (or the force) of the interaction, we can calculate the stresses necessary to cross these obstacles, as we did previously in the case of interaction between dislocations, either by the stress only (T=0 K) or due to thermal activation (T≠0 K).

8.5.2 Propagation of the dislocation through the distribution of point defects

Here, the problem is to analyze the dislocation motion through the distribution of obstacles interacting with it with the previously studied interactions. In the absence of thermal activation, $T = 0\ K$ the parameters involved in the gliding of the dislocation are (Fleischer model):

- the interaction force of the obstacle with the dislocation: $\boldsymbol{F_c}$
- the line tension (flexibility) of the dislocation: $\boldsymbol{\tau}$
- the spatial distribution of the obstacles, represented by their mean distance in the glide plane of the dislocation: $\boldsymbol{l}$

What we are trying to find is critical stress. σ_c

As in the case of the dislocation forest, the stress applied σ bends the dislocation between its obstacles with a radius of the curvature which - at equilibrium - is equal to:

$$R = \frac{\tau}{\sigma b}$$

The dislocation then has an angle of aperture ψ on the obstacle, depending simultaneously on R and the distance D between the obstacles along the dislocation line (Figure 8-18). The force applied on the obstacle by the line tension is then:

$$F = 2\cos\left(\frac{\psi}{2}\right)\tau$$

The obstacle is overcome when $F=F_c$, that is to say, when $\psi=\psi_c$ (critical escape angle), that is:

$$F_c = 2\cos\left(\frac{\psi}{2}\right)\tau = \beta\tau \qquad \text{with} \quad 0 < \beta < 2$$

The extremum values of β correspond respectively to:

- $\beta \approx 0$ or $\psi_c \approx \pi$, weak obstacles,
- $\beta \approx 2$ or $\psi_c \approx 0$, thus strong obstacles.

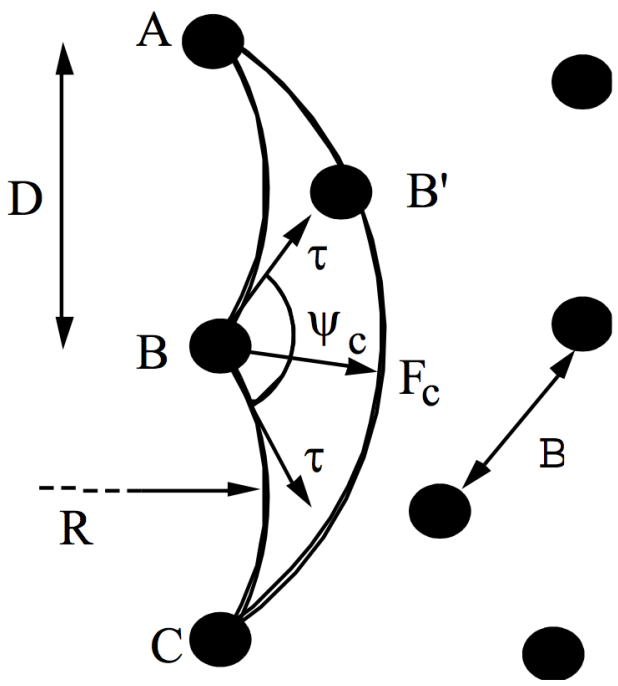

Figure 8-18: *Geometry of the overcoming of an obstacle by a bent dislocation*

The distance D between obstacles along the dislocation line varies, and the angles for a given stress also vary. The dislocation can unpin from all obstacles for which $\psi < \psi_c$ and impeded by others with $\psi > \psi_c$.

Figure 8-19 shows the results obtained by numerical simulation by Foreman & Makin (*Phil. Mag. 14 (1966) 911).*

Their approach was the following:

- a random configuration of points is chosen (stochastic generation), representing the distribution of impurities,
- the critical angle ψ_c is chosen, that is to say, the force of the obstacles (assumed of equal strength),
- we place a dislocation on the "starting line,"
- the external stress σ is increased (or R is decreased) by small incremental steps, and we measure ψ on each obstacle,
- if $\psi > \psi_c$, the portion of dislocation is not moved because the external stress is not sufficient to cross the obstacle,
- If, on the other hand, $\psi < \psi_c$, the portion of dislocation is displaced until the first obstacle for which $\psi > \psi_c$ and subsequent interactions.

The critical stress σ_c is then defined as the stress necessary for the dislocation to reach the other extremity of the distribution of obstacles. The results obtained from these simulations indicate that:

- for weak obstacles (Figure 8-19 a): the dislocation sweeps through defects on the plane
- for strong obstacles (Figure 8-19 b): the dislocation tends to widen in the least dense zones.

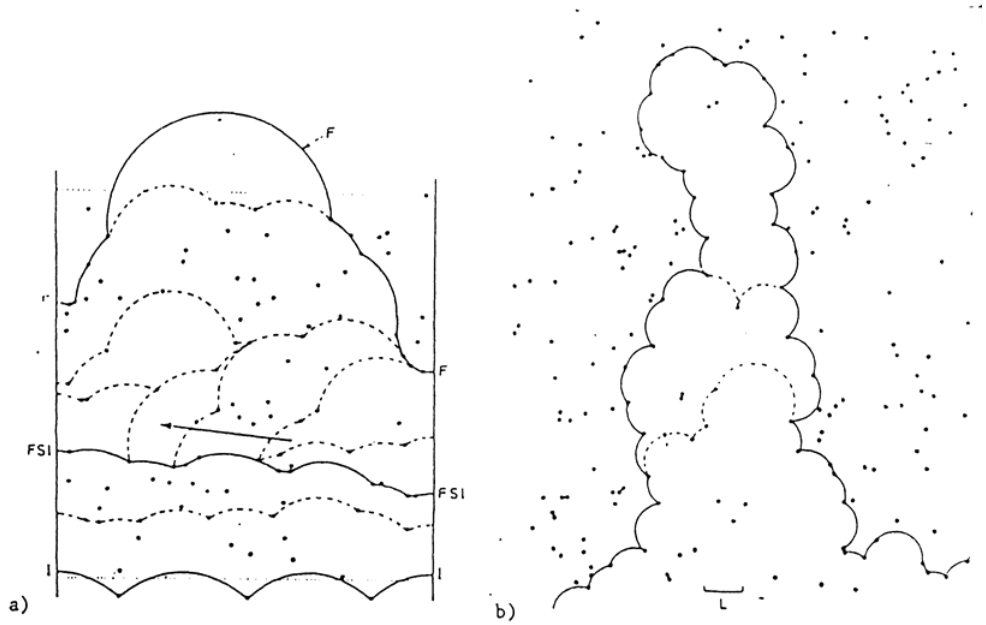

Figure 8-19: *Shape of a dislocation crossing weak obstacles a) and substantial obstacles b) according to the numerical simulations by Foreman and Makin*

8.6 Interactions with moving impurities

In the previous section, we described the interactions with impurities, assuming they are fixed. The dislocation encounters and has to overcome these pinning points to move. If the thermodynamic conditions allow it, the dislocation can also drag impurities. Such drag processes and conditions exist when the temperature is sufficient for the impurities to diffuse at a rate comparable to the dislocation glide velocity.

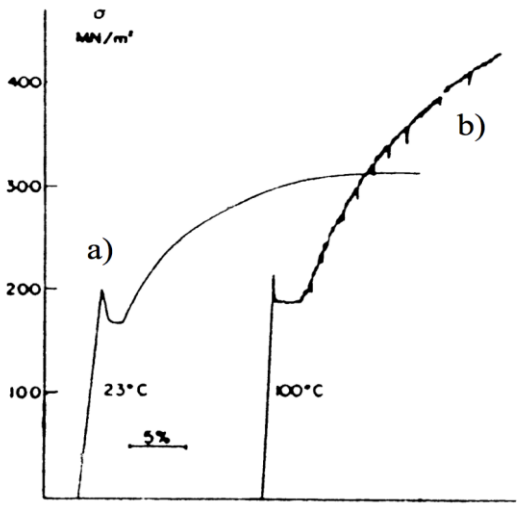

Figure 8-20 : *Strain curves in a Fe-C alloy. (a) Piobert-Lüders instabilities at the yield stress and (b) Portevin-Le Châtelier effect. The latter is characterized by an abrupt drop in the yield stress*

The interaction of impurities with dislocations and dragging impurities generate deformation instabilities. The two typical cases are the Piobert-Lüders slip bands (PL) (static aging) and the instabilities of Portevin-Le Châtelier (PLC). These are observed macroscopically, the deformation being unstable and heterogeneous.

The instability of Piobert-Lüders occurs around the elastic yield stress (Figure 8-20) and corresponds to:

- A low initial density of mobile dislocations, the existing dislocations being blocked by impurities diffusing to the core the dislocations,

- A catastrophic multiplication at the propagation front initiates in the zones where the stress concentration releases the dislocations from their traps.

8.6.1 Portevin - Le Châtelier effect (qualitative)

Unlike the PL instability, the PLC effect only appears after a critical deformation and repeats during the deformation process (see the strain curve in Figure 8-20).

This effect is due to dynamic aging characterized by two modes of dislocation velocity (Figure 8-21):

- In mode I (low velocities), the dislocations are sufficiently slow and drag impurities,
- In mode II (high velocities), the dislocations are much faster than the impurities, so these can be modeled as fixed obstacles for the dislocations.

In between these two modes, the slope of the stress $\sigma(v)$ as a function of the deformation speed is negative, which means that between the speeds v_1 and v_2, no stationary regime is possible for the dislocation. Thus, when the imposed deformation speed γ is such that the average dislocation velocity is either in regime I ($<v_1$) or II ($>v_2$), the deformation is, in principle, stable and homogeneous (Figure 8-21). On the other hand, when γ corresponds to the average speed of the dislocations between modes I and II, the PLC phenomenon occurs. At onset, dislocations move at velocities $<v_1$ in mode I, dragging their cloud of impurities (Figure 8-21).

The dislocations' velocities are insufficient to sustain the imposed deformation speed γ. Therefore, the stress applied σ increases until it reaches a value σ_1, where the dislocations are freed from their impurities cloud. The dislocations will then abruptly jump on branch II, where "fixed" impurities control their speed. In this mode, though, their speed is too high for the imposed deformation speed γ, and the stress decreases until $\sigma 2$, at which the dislocations are again sufficiently slow to be trapped by impurities. They then fall back into mode I, and this mechanism continually repeats and can often be experimentally observed as serrations on the stress-strain curve.

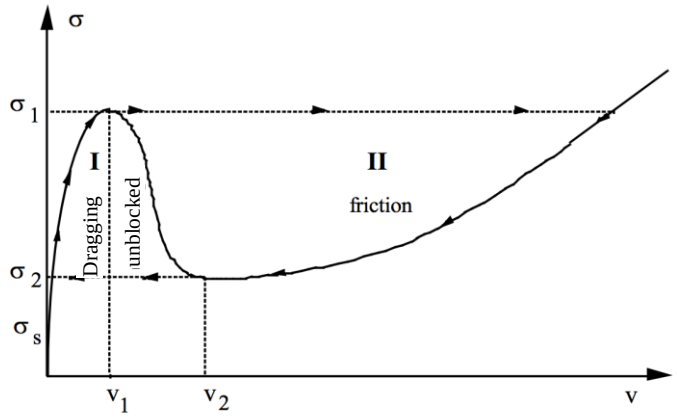

Figure 8-21: *Curve expressing the relation between stress and strain rate*

8.7 Interaction with precipitates

By simple gliding, i.e., in the absence of climb of dislocations or cross-slip, a dislocation can cross a distribution of obstacles of finite size only in two ways:

- by shear, if the precipitates are coherent with the matrix,
- by Orowan's bypass mechanism in all other cases.

8.7.1 Cutting of a precipitate

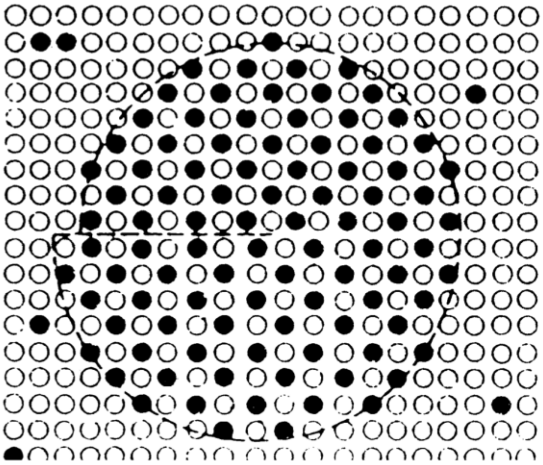

Figure 8-22: *Image of the Cutting of a precipitate at the atomic scale*

Consider a coherent precipitate cut by a matrix dislocation (Figure 8-22). For the sake of generality, we also suppose that the shear of this precipitate by the dislocation creates an interface with surface energy γ_p (e.g., in the case of ordered alloy precipitates).

The corresponding cutting mechanism requires the (Figure 8-22):

- the creation of an interface matrix-precipitate with surface energy γ_p
- the creation of an interface within the precipitate with surface energy γ_p

Calculating the critical stress σ_c requires specific details of the dislocation process that cuts the precipitates and is relatively complex and not presented here. Instead, we note the result obtained by Gleiter and Hornbogen (*Phys. Stat. Sol* ***12*** *(1965) 535)*, who expressed the critical stress as the shear between a pair of dislocations:

$$\sigma_c \sim \frac{\alpha \gamma_P^{2/3} f^{1/2} r^{1/2}}{\mu^{1/2} b^2} \tag{8.6}$$

It is important to note that the critical stress increases as the square root of the diameter of the precipitates.

8.7.2 Bypass mechanism

The bypass mechanism is the only possibility for dislocations to cross slip and glide around incoherent and coherent precipitates with high interphase or anti-phase energy if they are ordered alloy compounds. It is also possible to bypass the precipitate by climb, but Chapter IX deals with this topic in detail. In this case, the stress necessary for the cutting mechanism is so high that the dislocation bends between the precipitates until a semi-circular critical position is reached, in which adjacent dislocation line segments with opposing burger's vectors are in close proximity and annihilate. As a result, the dislocation line bypasses the precipitate, leaving around the precipitate a residual loop (Figure 8-24). This case is then an analog to a Frank-Read source.

For precipitates with planar mean radius in the glide plane *r* of the same size as the gap *D* (Figure 8-23) along with the dislocation, we have:

$$\sigma_c \approx \frac{\tau}{rb} \approx \frac{1}{2}\frac{\mu b}{r} \tag{8.7}$$

With $\tau \approx \frac{1}{2}\mu b^2$

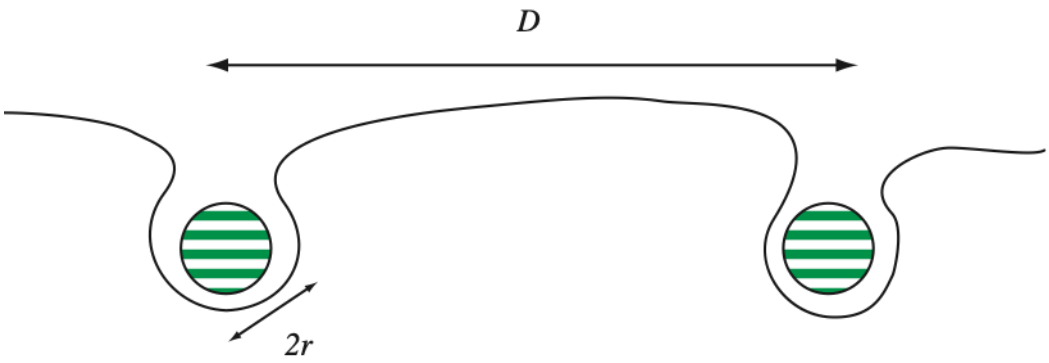

Figure 8-23: *Bypass mechanism of precipitates and formation of loops*

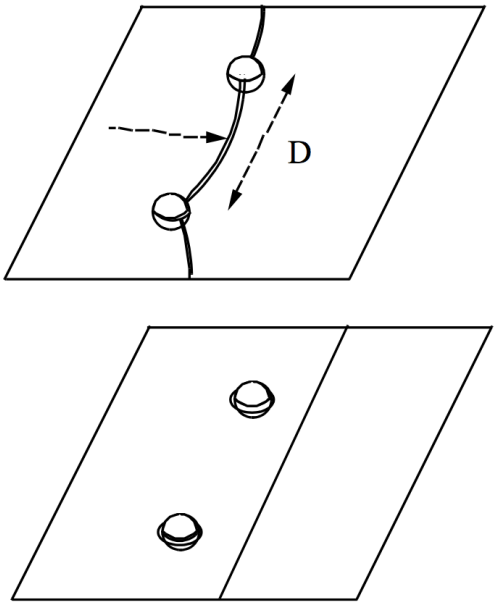

Figure 8-24 : *Overcoming of precipitates through bypass mechanism. The dislocation encircles the precipitate and leaves behind it a loop around the precipitate*

If the radius of the precipitates is small with respect to the distance *D* between them, this becomes the critical parameter. The critical radius of curvature is *D/2*, thus:

$$\sigma_c = \frac{2\tau}{Db} \approx \frac{\mu b}{D} \qquad (8.8)$$

called the critical Orowan stress (*D* either being a function of σ or assumed independent).

In the case of coherent precipitates, with constant volume fraction *f*, the radius *r* of the precipitates is proportional to *D*, the mean distance between the precipitates in the glide plane:

$$D \sim \sqrt{\frac{\pi}{f}} r$$

We obtain then:

$$\sigma_c = \frac{2\tau f^{1/2}}{\sqrt{\pi} rb} \qquad (8.9)$$

8.7.3 Competition between the Bypass and Cutting mechanisms

The critical stress σ_c for the bypass mechanism and the Cutting grows as *1/r* and $r^{1/2,}$ respectively (formulas (8.6) and (8.9)). Thus, the crossing occurs for a constant volume fraction *f* and a given radius *r* when the lower critical stress mechanism reaches its threshold.

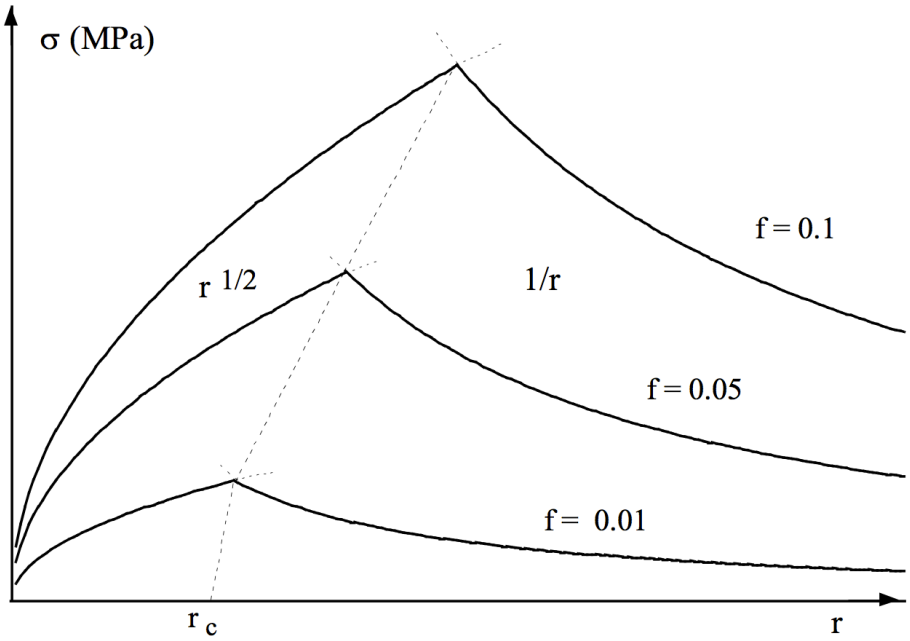

Figure 8-25: *Yield stress as a function of the radius of precipitates. Change from the Cutting to the bypass mechanism*

We can see that (Figure 8-25) at a constant volume fraction of precipitates *f*, in a structure with large precipitates (i.e., with significant gaps and large precipitates), dislocations glide via a bypass mechanism. In contrast, dislocations propagate by cutting precipitates in a structure with small precipitates (i.e., closer together). Generally, the critical radius r_c separating the two behaviors depends slightly on *f* and corresponds to a hardening thermal treatment, which is material-specific and corresponds to the largest flow stress that this kind of precipitate can obtain.

8.8 Interaction with the grain boundaries: Hall-Petch law

In polycrystalline materials, the path of dislocations is also limited by the interfaces formed by grain boundaries. The experimental measures often show a dependency of the elastic yield stress on the size of the grains *d*:

$$\sigma_y = \sigma_0 + k_y d^{-0.5} \tag{8.10}$$

This behavior has been justified by Hall and Petch (*E.O. Hall, Proc. Phys. Soc.* ***B64****, (1951) 747 and N. J. Petch, Phil. Mag.* ***3*** *(1958) 1089)* by the piling up of dislocations at the grain boundaries. In this model, the stresses of the dislocations accumulated at the grain boundary must be sufficient to cause other sources in the adjacent grains.

Considering a source S_1 in the grain 1 (Figure 8-26) and a shear stress on the glide plane τ, we can show (*Eshelby J. D., Frank F. C., Nabarro F. R. N. Phil. Mag.,* ***42*** *(1951) 351)* that the stress near the leading dislocation τ_1 depends on the number of dislocations in the pile-up and on the shear stress applied: $\tau_1 = n\tau$.

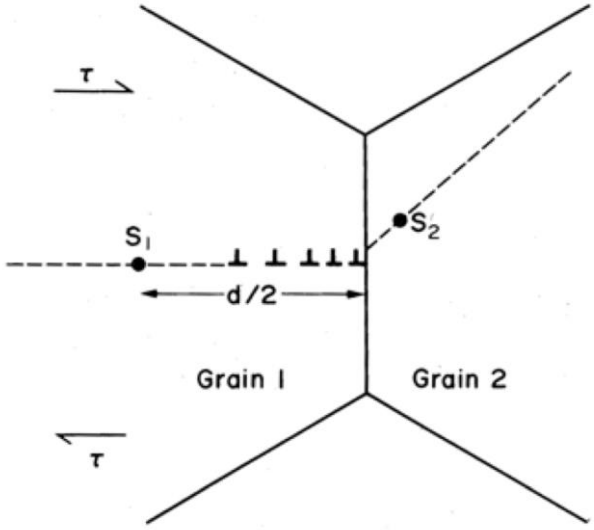

Figure 8-26: *Diagram of the dislocations coming from a source S_1 piling up at the joint between grains 1 and 2. The stresses due to the pile activate the source S_2*

We use the expression of the repulsive force between two dislocations with the same sign (7.32) and consider a force balance at equilibrium. If *n* dislocations pile up on the same glide plane, for the n^{th} to move (Figure 8-26), the stress applied must be:

$$\tau = \frac{\mu b^2}{\frac{2\pi(d/2)}{n}} = n\frac{A}{d} \tag{8.11}$$

Since : $n = \frac{\tau_1}{\tau}$

$$\tau_1 = \frac{d}{A}\tau^2 \tag{8.12}$$

If we assume that the source S_2 in grain 2 has begun to operate when the stress at the boundary takes a critical value τ^*_1, then:

$$\sigma_y \propto \tau = \sqrt{\frac{A}{d}\tau_1^*} = k_y d^{-0.5} \tag{8.13}$$

with $k_y = m^{-1}(A\tau_1^\star)^{1/2}$, where *m* is the Schmid factor.

The Hall-Petch relation is obtained, assuming that the dislocations generated by S_2 move under the action of a friction force σ_0. One could notice that the distance among dislocations in the pile-up is proportional to the distance from the grain boundary, as represented in Figure 8-26. This is also observed experimentally. Figure 8-27 shows pile-ups of dislocations against a grain boundary in pure Cu using the etch pit analysis technique.

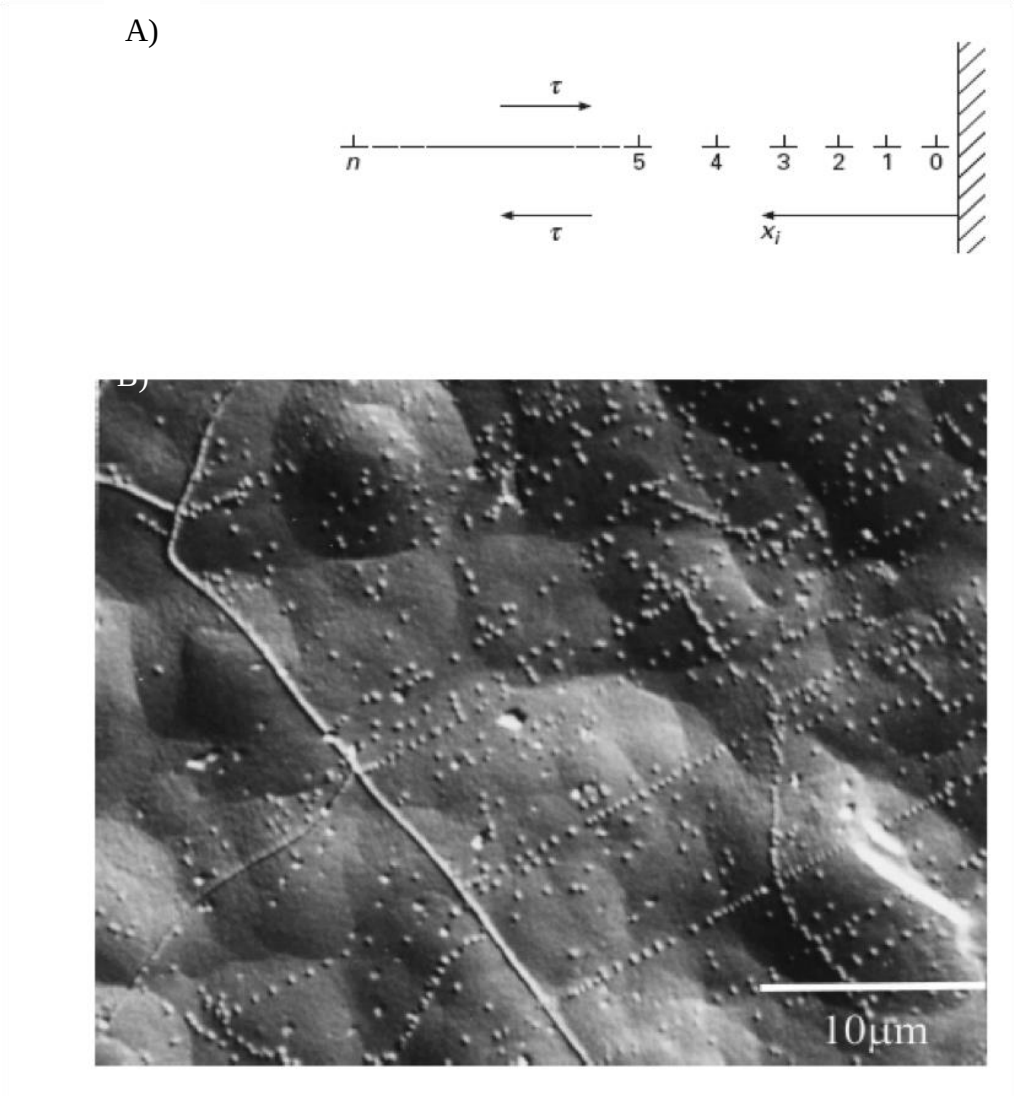

Figure 8-26: *A) Diagram of the dislocation pile-up distance and B) image of Cu surface etch pitted to show their*